Characterization and long term operation of a novel superconducting undulator with 15 mm period length in a synchrotron light source

S. Casalbuoni,[*] A. Cecilia, S. Gerstl, N. Glamann, A. W. Grau,
T. Holubek, C. Meuter, D. Saez de Jauregui, and R. Voutta

Karlsruhe Institute of Technology, P.O. Box 3640, D-76021 Karlsruhe, Germany

C. Boffo, Th. Gerhard, M. Turenne, and W. Walter

Babcock Noell GmbH, Würzburg 97080, Germany

A new cryogen-free full scale (1.5 m long) superconducting undulator with a period length of 15 mm (SCU15) has been successfully tested in the ANKA storage ring. This represents a very important milestone in the development of superconducting undulators for third and fourth generation light sources carried on by the collaboration between the Karlsruhe Institute of Technology and the industrial partner Babcock Noell GmbH. SCU15 is the first full length device worldwide that with beam reaches a higher peak field than what expected with the same geometry (vacuum gap and period length) with an ideal cryogenic permanent magnet undulator built with the best material available PrFeB. After a summary on the design and main parameters of the device, we present here the characterization in terms of spectral properties and the long term operation of the SCU15 in the ANKA storage ring.

I. INTRODUCTION

An undulator is an array of dipole magnets with alternating magnetic field direction. When placed in a synchroton light source, the ultrarelativistic electrons stored in the accelerator are guided by an undulator onto a quasisinusoidal path producing highly collimated photon flux. The state of the art technology for these devices is based on permanent magnets. A number of techniques have been developed and applied in the last years to increase the magnetic peak field on axis for a fixed period length, which allows us to increase the spectral range and the brilliance. In order to maximize the peak magnetic field on axis for a certain period length, the magnetic gap needs to be minimized. This is obtained by keeping the permanent magnets in vacuum, reducing the difference between vacuum and magnetic gap. To further increase the peak field on axis, the magnets can be cooled. A possibility to reach higher magnetic peak fields on axis than the ones obtainable with cryogenic permanent magnet undulators (CPMUs) is to use superconducting magnet technology, which has been and is widely applied in particle accelerators.

Several facilities worldwide have been and are working on the development of superconducting undulators (SCUs)

[1]. The development of superconducting undulators started in Karlsruhe in the early 1990s [2]. A first superconducting undulator demonstrator with 14 mm period length and 100.5 periods SCU14DEMO (developed in collaboration with Accel GmbH) was installed and operated in the ANKA storage ring from 2005 to 2012 [3]. The performance of this demonstrator device, in particular the magnetic peak field on axis was limited by the beam heat load to a smaller value than the one obtainable with permanent magnet undulators. At the Advanced Photon Source (APS), a 0.3 m short prototype with a period length of 16 mm and 20.5 periods has been successfully tested with beam, reaching a peak field on axis up to 0.8 T with a beam vacuum gap of 7.2 mm and a magnetic gap of 9.5 mm [4].

The Institute for Beam Physics and Technology (IBPT) at the Karlsruhe Institute of Technology (KIT) and the industrial partner Babcock Noell GmbH (BNG) are developing superconducting undulators for the current and the next generation low emittance light sources using NbTi as superconducting wire, the working horse of superconducting magnets applied in particle accelerators. The systems are conduction cooled and have a variable gap. Conduction cooling is realized by employing cryocoolers, requiring only water and electricity to operate. No liquid helium (LHe) or nitrogen is needed to cool these undulators. These features are user friendly and particularly convenient for all the facilities without a helium recovery system. ANKA has no full energy injector, and the beam energy is ramped, after having injected all the current, from 0.5 GeV to 2.5 GeV. This requires the developed devices to have a
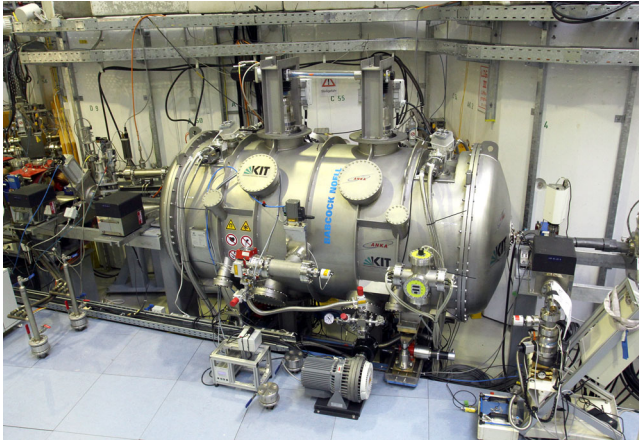
[*]sara.casalbuoni@kit.edu

FIG. 1.   SCU15 installed in the ANKA storage ring.

minimum vacuum gap of 7 mm at full energy, in order not to reduce the electron beam lifetime, and one of 15 mm at injection. Thus, an adjustable gap is needed. All the SCUs under development for other facilities have a fixed gap [1], which reduces the complexity in terms of design, manufacturing and assembly. However, the variable gap is a standard feature for permanent magnet undulators being highly desirable during commissioning and "nice to have" during operation, especially for small gap devices as employed in low emittance light sources (vacuum gap down to 4–5 mm).

As a significant milestone of the collaboration between KIT IBPT and BNG a SCU with 15 mm period length (SCU15) and 100.5 periods has been tested for one year in the ANKA storage ring (see Fig. 1). The SCU15 reaches a magnetic peak field on axis of 0.73 T with a vacuum gap of 7 mm and a magnetic gap of 8 mm. This is the result of an aggressive design focused in reducing the difference between magnetic and vacuum gap to 1 mm. As a comparison, the SCU prototype developed and tested at APS has a difference in gap of 2.3 mm. The value of the peak field on axis reached by the SCU15 is about 16% higher than the one [5] achievable with a CPMU using PrFeB (best material available) with the same geometry (7 mm vacuum gap and 15 mm period length), and not yet demonstrated experimentally.

In this paper we first summarize the design and the key parameters of the SCU15, we report on the main results obtained during the cold tests without beam, on the operation and finally on the spectral characterization of the SCU15 in the ANKA storage ring.

II. SCU15 LAYOUT

A scheme of the SCU15 is presented in Fig. 2. The coils are embedded in the insulation vacuum and connected to external motors, which allow us to change the vacuum gap. The magnetic gap at room temperature is fixed by a spacer machined to a precision of ± 0.01 mm. In operating conditions (cold), after thermal contraction, the magnetic
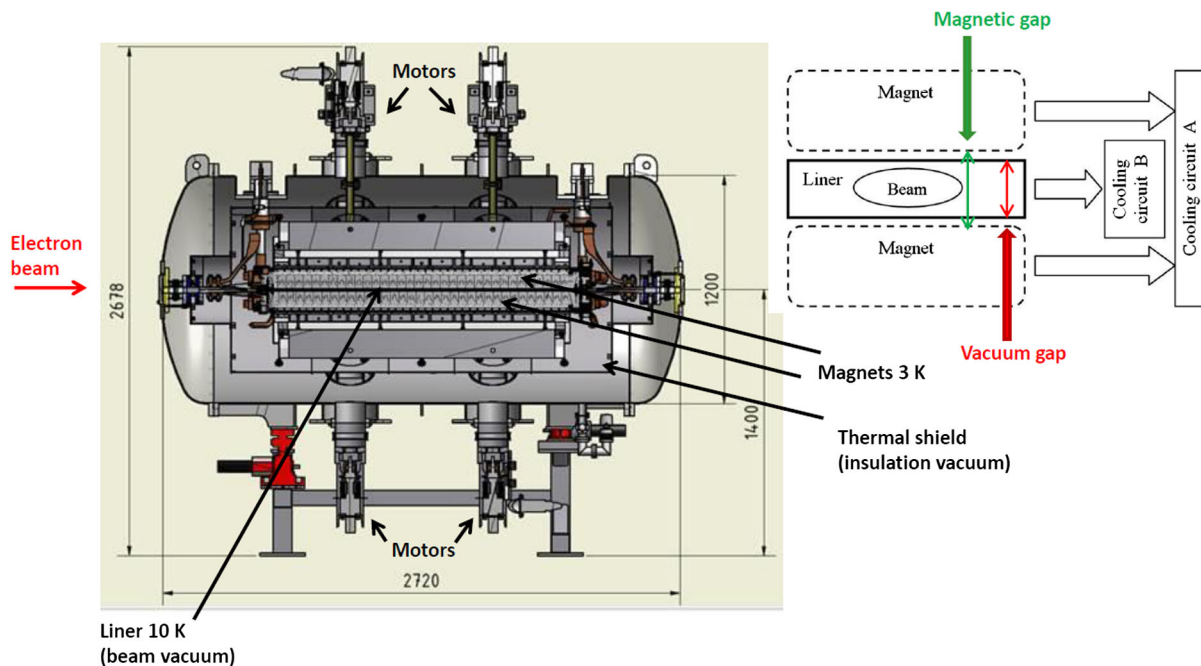

FIG. 2.   On the left, a scheme of the SCU15 indicating the beam vacuum chamber (liner), the magnets embedded in the insulation vacuum, and the motors used to change the vacuum gap, is shown. On the right side, a scheme of the separate cooling circuits cooling the magnets (cooling circuit A) and the liner (cooling circuit B) allowing a good thermal separation between magnets and coils, as well as the difference between magnetic and vacuum gap, is presented. The dimensions shown are all indicated in mm.

TABLE I.   Main parameters of the SCU15.

Average period length	15.01 mm
Number of fully wound periods	100.5
Operating max. peak field on axis	0.73 T
Operating max. current	150 A
Magnetic gap closed	8 mm
Vacuum gap closed	7 mm
Vacuum gap open	15 mm
Design beam heat load	4 W

TABLE II.   Mechanical accuracies of the two undulator coils reached at room temperature.

Winding height accuracy	40 μm
Pole height accuracy	50 μm
Half period length accuracy	35 μm

gap is calculated to be 8.00 ± 0.01 mm. A good thermal separation between magnets and liner can be obtained by using 2 separate cooling circuits for the magnets (cooling circuit A) and the liner (cooling circuit B), as well as by avoiding physical contact between magnets and liner all along the magnets length (magnetic gap > vacuum gap). The key parameters of the SCU15 are summarized in Table I. The average period length of the SCU15 is 15.01 mm (over 100 periods) and the maximum peak field on axis 0.73 T for a vacuum gap of 7 mm.

Each coil is made by a rectangular NbTi wire (0.54 mm x 0.34 mm) wound on a yoke built of 206 cobalt-iron alloy plates aligned and pressed by two stainless steel rods. Each plate consists of a pole and a winding groove. The rectangular shape of the superconducting wire allows us to maximize the engineering current density. The full winding packages have 7 single turns on 13 layers. In order to minimize the first and second field integrals, the first and second end winding packages have 7 single turns on 3 layers and on 9 layers, respectively. As a result of a repair on the coils during assembly, which required the bypassing of the windings in the last groove of one coil, the first and second field integrals are not compensated. Helmholtz coils wound with a 0.229 mm diameter NbTi wire on an aluminum former and positioned at the entrance and exit of the magnet, have been included with the aim of reducing the vertical first I_1 and second field integral I_2 below the values needed for the device to be transparent to the electron beam: $|I_1| < 3 \times 10^{-5}$ Tm and $|I_2| < 4 \times 10^{-4}$ Tm^2. With the available cooling, each pair of Helmholtz coils can sustain a current of 1 A and correct a first field integral of $I_1 = 1.3 \times 10^{-3}$ Tm.

A passive quench protection system based on cold diodes is applied to the magnet. Quench detection is implemented in the main power supply, and triggered by the voltage difference across the two coils.

The spectral performance of an undulator depends on the field quality. The highest intensity of the undulator radiation is reached by the constructive interference of the photons emitted at each pole at specific wavelengths:

$$\lambda_n = \frac{\lambda_U}{2n\gamma^2}\left(1 + \frac{K^2}{2} + \theta^2\gamma^2\right) \qquad (1)$$

where λ_U is the period length of the undulator, n is the harmonic number, γ is the Lorentz factor, θ is the observation angle, and $K = 93.36B_0\lambda_U$ is the so-called deflection parameter with B_0 being the peak field on axis in T and λ_U in m. If the field quality of the magnetic field is poor (different λ_U and B_0 at each period), the width of the harmonics increases and consequently their height decreases lowering the radiation intensity at the specific wavelengths.

The field quality of a SCU is strongly determined by the geometrical precision reached in operating (cold) conditions. Thus, it is essential to reach a high geometrical precision at room temperature. A more detailed description of the magnet fabrication is provided in Ref. [6]. The mechanical accuracies measured at room temperature are within 50 μm, as shown in Table II. All values shown are measured with a coordinate measuring machine (CMM) with the exception of the winding package position accuracy, which has been estimated from the deviation of the diameter dimension of the superconducting wire (3 μm). The pole height and the half period length values reported in Table II are the difference between the maximum and minimum measured value. The plates, which have a thickness precision within 20 μm, have been sorted to minimize the accumulation of the half period length inaccuracies, so that a maximum deviation from the ideal value of the pole longitudinal position of 35 μm is achieved. The overall difference in length between the two coils is 20 μm.

The superconducting coils are impregnated with epoxy resin and for this reason they are not compatible with the ultra high vacuum needed for the beam. The beam vacuum chamber is a flexible liner made of a 0.3 mm stainless steel foil, which separates the beam vacuum from the isolation vacuum of the superconducting coils. In case of a leak in one of the two vacuum systems, the liner is able to sustain a pressure difference of 1 bar. The liner allows a change in beam stay clear from 15 mm to 7 mm, and in order to reduce the resistive losses induced by the electron beam, it is coated with a 30 μm thick copper layer.

The superconducting undulator coils are designed to operate at 173 A at about 4.2 K with 30% margin on the load line. In order to cool the whole system 4 cryocoolers are used: 2 Sumitomo RDK415D [7] providing each at the second stage 1.5 W at 4.2 K to cool the magnet and 35 W at 50 K at the first stage for the current leads and the thermal shield, and 2 Sumitomo RDK408D2 providing 4.0 W each at 10 K at the second stage to cool the liner and the support

structure of the magnet and 40 W each at 50 K to cool the thermal shield. The heat is transported via high thermal conductivity copper braids. A design value of 4 W, inferred from the beam heat load estimated from the measurements performed with the SCU14DEMO [8], has been assumed for the heat on the liner due to the interaction of the beam with the surrounding vacuum chamber. A significant technical challenge, solved with the SCU15, is to maintain the thermal separation between the liner at about 10 K and the magnet at around 4 K, minimizing the distance to about 0.2 mm over a surface of 0.15 m^2 along 1.5 m.

III. COLD TESTS

Before assembling the SCU15 coils in the final cryostat, they have been tested in a LHe bath cryostat at CERN. The results of the training and local field measurements are reported in Ref. [9]. During training 2 failures have been found and successfully repaired. In one case it was found that the wire was burned on a length smaller than 0.5 mm. In the second case the failure is believed to be due to a defect of about 50 μm on the winding groove, which caused a partial burn of the wire after quenching. In the end the magnet reached a plateau at 157 A. An operation point at 150 A and 3.5 K allows for a 20% margin on the loadline. For the test, the SCU15 coils were mounted in a stainless steel support structure fixing the magnetic gap at room temperature at 8.00 ± 0.01 mm. After cooldown the magnetic field measurements showed that each coil bent about 250 μm, increasing the magnetic gap toward the two ends. This is believed to be due to the different thermal contraction of the coils and of the stainless steel support structure. In order to compensate this bending, before installing the coils in the final cryostat, they have been pre-bent in the opposite direction at room temperature. The SCU15 coils magnetic field profile has not been measured after installation in the final cryostat.

Several tests have been performed before installation of the SCU15 in the ANKA storage ring as well as after installation without beam. Cooldown and warm up times of approximately 7 and 4–5 days are achieved. It is important to keep the duration of cooldown and warm up of the device shorter than 1 week in order to cope with reasonable shutdown times of the accelerator, during installation and maintenance. Maintenance of the cold heads of the cryocoolers is needed, according to their manufacturer, every 10 000 h of operation, which means that the device needs to be warmed up once per year. The cooldown time is demonstrated in Fig. 3, where the temperatures of the SCU15 coils (top and bottom) as well as the temperature of the liner are shown after installation in the storage ring. The lowest temperature reached by the liner is 10 K, while the superconducting coils reach between 3.1 K and 3.2 K (below 10 K the typical accuracy of the sensors is below 10 mK). The temperature sensors on the coils are located in the middle of the magnet, which is the farthest point from
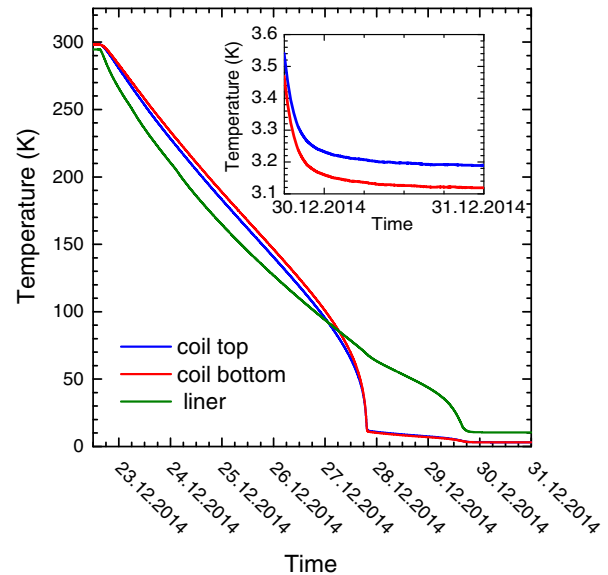

FIG. 3. Cooldown time of the SCU15. The temperature of the superconducting coils are plotted as well as the temperature of the liner as a function of time. In the inset the lowest temperature reached by the SCU15 coils is shown.

the cryocooler cold head along the cooling connection, representing therefore the so-called hot spot (warmest region in the magnet). The temperatures of the SCU15 superconducting coils and of the beam vacuum chamber are shown in Fig. 4 as a function of time during the warm up procedure. In order to warm up the device the cryocoolers are first stopped, then the heaters placed on the coils are powered until the temperature of the liner reaches around 80 K. Afterward, the heaters are turned off and nitrogen gas
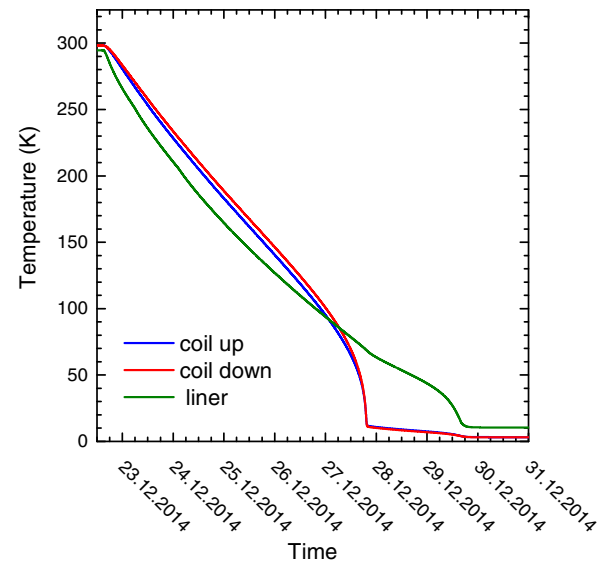

FIG. 4. Warm up time of the SCU15. The temperature of the superconducting coils are plotted as well as the temperature of the liner as a function of time.
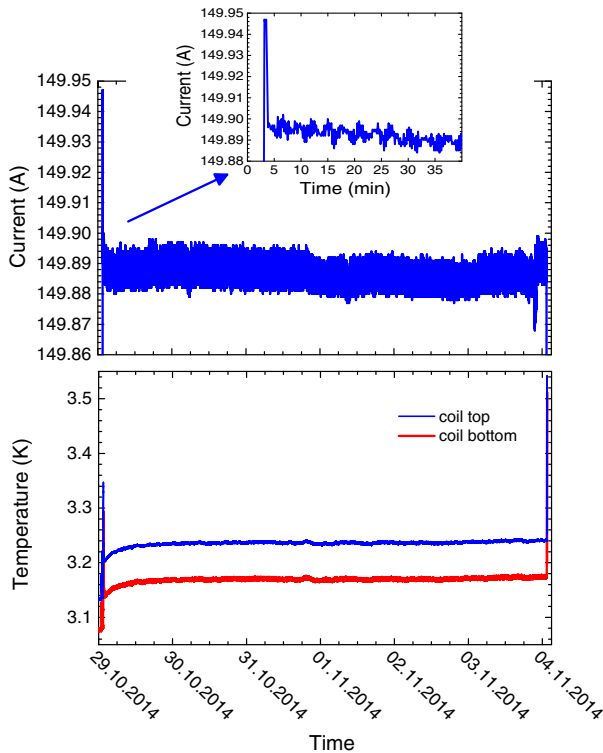
FIG. 5.   Upper plot: current of the power supply feeding the main superconducting coils at the maximum operating current as a function of time; the inset shows the stability during the first 30 min after ramping. Lower plot: temperature of the superconducting coils reported as a function of time.

is introduced. The warm up time can be reduced down to about 4 days by increasing the pressure of the nitrogen gas.

After cooldown the isolation vacuum of the SCU15 is about 2×10^{-9} mbar, while the beam vacuum reaches 10^{-11} mbar. The beam vacuum of the SCU15 to which we refer to is measured as follows, before installation of the SCU15 in the storage ring. On one side the liner was pumped, while a baked and pumped cross with a pressure gauge and a residual gas analyzer (RGA) was installed on the other side. The vacuum of the cross was separated by an all metal valve from the vacuum of the SCU15 beam chamber. Before cooldown the all metal valve was closed and the pressure in the cross was 10^{-11} mbar. After cooldown the valve was opened and the pressure gauge did not show any change in pressure. We point out that 10^{-11} mbar is the minimum pressure value measurable with the pressure gauge used (Penning IKR70). The measurement of the residual gases after opening the all metal valve confirms the cleanliness of the SCU15 beam vacuum chamber: the signals of all masses scanned from 1 to 78 are below the instrument resolution.

Figure 5 shows the current of the power supply feeding the main superconducting coils at the maximum operating current and demonstrates the stability of the device tested for 6 days, during which no quench occurred. During the
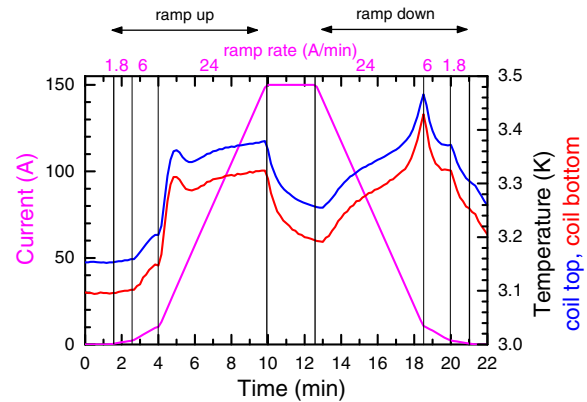

FIG. 6.   Current of the power supply while ramping up and down the main superconducting coils (left axis) and temperature of the top and bottom coils (right axis) as a function of time.

first minute after that the magnet is ramped, a variation of the current of about 4×10^{-4} is observed (see inset of Fig. 5). Afterward, the current stays constant within 2×10^{-4} for the next 6 days. During this time, the maximum temperature of the coils is 3.25 K, while without current in the magnet it is 3.12 K. This increase in the temperature is due to the additional heat load generated in the current leads when the magnet is energized. As reported in Fig. 6, no relevant temperature increase of the magnet is shown during the minimum ramp time of 450 s. The ramp rate is set to lower values, indicated in Fig. 6, when the main current is lower than 10 A, in order to keep the quench detection window constant to 100 mV in 100 ms. The increase in temperature during ramp of the magnet is generated by hysteresis in the superconducting wire and iron yoke, and by coupling losses in the superconducting wire.

The magnet can be energized only when the gap is closed. It is therefore important that no temperature increase takes place while closing the gap. When the beam stay clear is closed from 15 mm to 7 mm, the thermal connection of the coils and of the liner to the outer cryostat
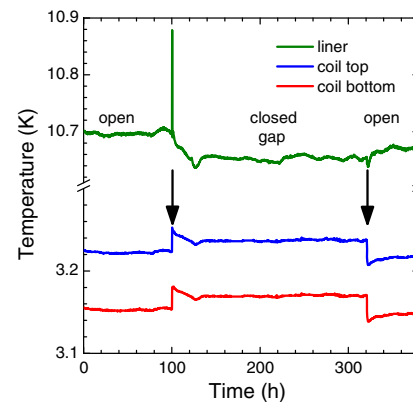

FIG. 7.   Temperature of the SCU15 coils and of the liner as a function of time with gap closed and open.

improves and a slight temperature increase is observed, as shown in Fig. 7. The observed temperature transient in the coils while closing the gap is however negligible for operation purposes.

IV. ALIGNMENT

Another big challenge of a cryogenic undulator is the alignment. As for permanent magnet undulators, vertical alignment is needed in order to minimize the horizontal (longitudinal) component of the magnetic field seen by the electrons, which is for a perfect device zero only in the middle of the undulator gap. Alignment in the horizontal direction is relevant for all undulators to ensure that the electrons go through the good field region, and to protect the undulator from the synchrotron radiation of the upstream bending magnet. Furthermore, for superconducting undulators alignment is extremely important to minimize the beam heat loads. The magnet axis and plane need to be referenced with a precision of few $100~\mu m$ to the fiducial points out of the cryostat. The alignment procedure of the SCU15 was performed at room temperature. There is no method known to the authors applicable while the magnet is cold. Because of this, the system is designed to avoid shifts of the magnetic plane after cooldown.

Each coil is mounted on a strong-back connected to a motor through 2 titanium alloy rods. The motors moving the top and bottom coils are synchronized, and allow the change of magnetic gap from 16 mm to 8 mm. The distance between the coils is fixed by a spacer, which is connected to the outer cryostat by 8 titanium alloy rods, supporting the magnet at each end. These connections are designed to allow keeping the magnet plane fixed after cooldown. The concept has been tested by placing a precision piece with a well-defined edge in the beam vacuum chamber. The position of the edge was measured unchanged before and after cooldown. The measurement has been performed with an optical level Leica NA2 (accuracy about $30~\mu m$) looking through a quartz window mounted on the cryostat at one end of the beam vacuum chamber.

The position of 3 points on the first and last poles of each coil was referenced to 4 fiducials placed in pair on the coils end plates by using a CMM. The point in the middle of each pole (along the x axis, see Fig. 8) is used to define the magnetic axis, while the other 2 are placed at 20 mm on the left and right. After that the coils are aligned to each other, each point on the upper pole at each end is connected to the corresponding point on the lower pole, as indicated in the sketch shown in Fig. 8. The middle points of each of these segments are used to define the magnetic plane, while the magnetic axis is defined by the line connecting the middle points at the beginning and at the end of the magnet. The magnetic axis and plane are then referenced to the 8 fiducial marks on the coils. After installation of the superconducting coils in the cryostat it is possible to reference the 8 fiducial marks on the coils to the 4 fiducial marks on the
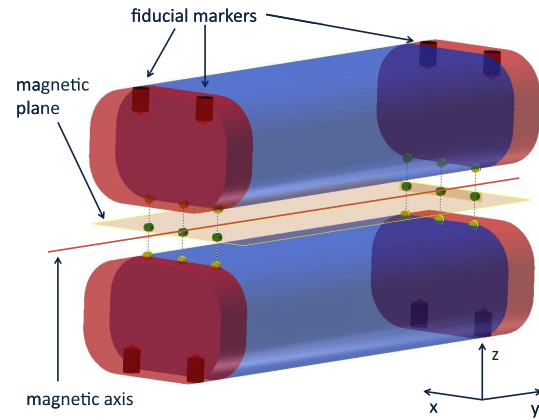

FIG. 8. Sketch of the superconducting coils with the fiducials, the points used on the first and last poles, as well as with the magnetic plane and axis.

cryostat with a laser tracker. The position of the magnetic axis at room temperature with respect to the 4 fiducial marks on the cryostat has been determined with a precision of ± 0.1 mm vertically and ± 0.2 mm horizontally.

The alignment of the SCU15 in the ANKA storage ring was performed with a laser tracker using the 4 fiducials on the cryostat with a precision of ± 0.15 mm vertically and horizontally.

V. OPERATION IN THE ANKA STORAGE RING

The most relevant achievement of the SCU15 is that the beam heat load does not limit the peak field on axis, allowing us to reach a peak field higher than what obtainable with competing technologies (as already mentioned in Sec. I). This result confirms that it is possible to reduce the difference in magnetic gap and beam stay clear to 1 mm while keeping a good thermal decoupling between the liner and the coils (see Fig. 9). This was not the case in the SCU14DEMO, where the liner and the coils were in thermal contact. The stable operation of the SCU15 at the maximum current of 150 A has been demonstrated. This allowed a reliable operation of the ANKA storage ring, without being affected by any quench of the SCU15 during operation at 2.5 GeV electron beam energy. As an example, Fig. 9 shows the current in the main coils, the corresponding temperature of the top and bottom magnets, and the temperature of the liner. The beam parameters (current, energy, and lifetime) are shown in the plot on the bottom.

In a machine like ANKA working in current decay mode it is very important to keep the lifetime as long as possible. During the tests, the SCU15 was the device with the smallest vertical gap installed in ANKA. As shown in Fig. 10, the lifetime was not affected by operating the SCU15, meaning closing the vertical gap and powering the superconducting coils. A reduction in lifetime is expected for vacuum gaps smaller than 7 mm, and in presence of higher order magnetic field multipoles. The operation of
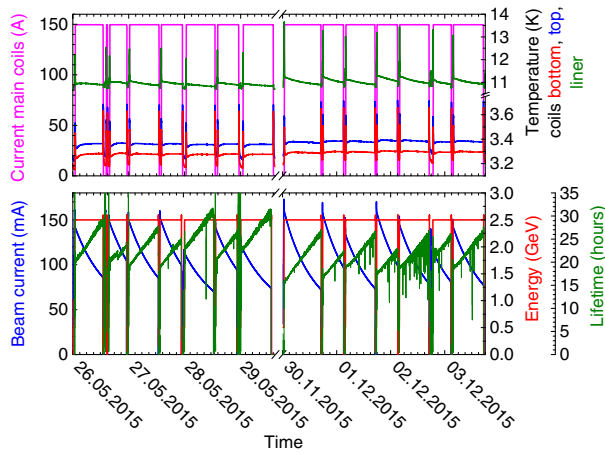
FIG. 9. Top. Current of the main coils (magenta line) of the SCU15 and the temperature of the top (blue line) and bottom (red line) coils, as well as the temperature of the liner (green line), as a function of time. Bottom. Beam parameters as a function of time: current (blue line), energy (red line), lifetime (green line).

the SCU15 does not affect the lifetime, except in the first three minutes after that the gap is closed. This effect is caused by the falling of the cryosorbed gas from the wall of the cold vacuum chamber, the interaction of which with the electron beam generates the observed pressure increase. This is also a relevant result for the application of SCUs to low emittance light sources.

A comparison of the beam lifetime in the ANKA storage ring before and after installation of the SCU15 is shown in Fig. 11. The SCU15 is here with gap closed and powered to 150 A. The data shown after installation of the SCU15 are after conditioning, which was necessary after venting

FIG. 11. Reported are the beam current (blue), the beam energy (red), and the beam lifetime (green) as a function of time before and after installation of the SCU15 in the ANKA storage ring. The SCU15 is here with gap closed and powered to 150 A.

the 5 m long straight section. As shown in Fig. 12, after 10 days of conditioning, operating at 2.5 GeV the beam lifetime at 100 mA beam current was about 15 hours. The 23 hours lifetime at 100 mA have been recovered after about 30 A h integrated current (considering only operation at 2.5 GeV).

After installation of the SCU15 in the ANKA storage ring, and after its cooldown, the UHV pressure could be measured by the readout of the ion pumps placed in the warm vacuum chambers, about 1 m long, located upstream and downstream with respect to the SCU15. The upstream chamber was baked before installation, while the baked downstream chamber had to be exchanged with an unbaked one, due to the presence of a leak. The static pressure before beam operation was 5×10^{-10} mbar and 7×10^{-10} mbar,
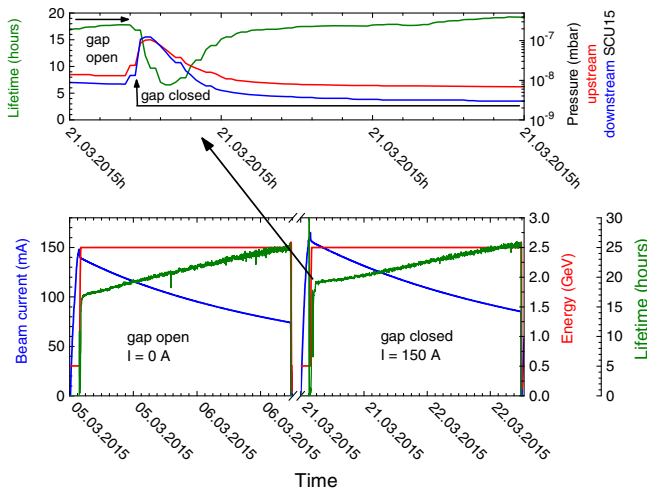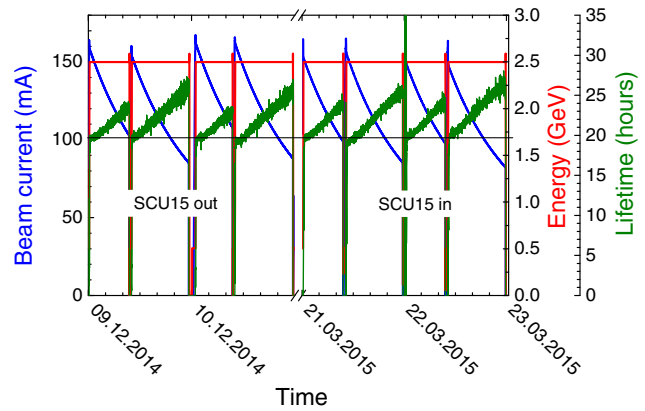

FIG. 10. Top. Lifetime and pressure measured in the vacuum chambers at room temperature placed upstream and downstream with respect to the SCU15, as a function of time when the gap is closed. Bottom. Beam parameters as a function of time: current (blue line), energy (red line), lifetime (green line).
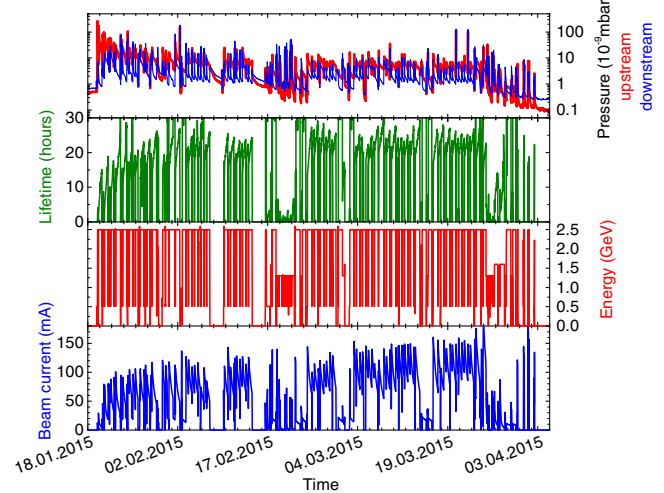

FIG. 12. Pressure in the vacuum chambers upstream and downstream with respect to the SCU15, beam current, beam energy, and beam lifetime as a function of time after installation of the SCU15 in the ANKA storage ring.

respectively. Figure 12 shows the evolution of the UHV pressure measured in the vacuum chambers located upstream and downstream with respect to the SCU15 for the first 2.5 months of operation as a function of time (upper plot) as well as the beam energy, current, and lifetime in the lower plot. Vacuum conditioning is reached after about 1 month of beam operation.

As anticipated in Sec. II, as a result of a repair of the coils during assembly, the windings of the last groove of the top coil have been bypassed, with the consequence that the first and second field integrals are not compensated. This asymmetry in the end fields introduces a constant magnetic field all along the SCU15 main coils, causing a bending of the electron trajectory. The Helmholtz coils placed at the entrance and exit of the SCU15 magnetic structure, due to the available cooling, can sustain only a current of 1 A instead of the foreseen 7 A and cannot compensate the field integrals introduced by the uncompensated end field configuration. The SCU15 could be however operated by using, during the first months after its installation, the orbit correction of the ANKA storage ring, and later on an additional ANKA horizontal corrector installed upstream. The corrector current was changed only together with the current of the main coils of the SCU15 to compensate a maximum first field integral of 2.5 T m. While changing the undulator current (tuning) the WERA (Weichröntgen-Analytik-Anlage) beam line, which is the most sensitive to intensity changes has measured intensity variations of about 1% [10]. This result can be further improved by optimizing even more the orbit correction.

The SCU15 operated safely for one year without quenches during the 2.5 GeV runs. Only 2 quenches happened in the test period with beam, while operating ANKA at 1.3 GeV to reach the low α_c momentum compaction mode [11], after the electron beam loss. As can be seen in Fig. 13 the electron beam current drops to 0 A, and the temperature of the coils starts to increase. After a few seconds a quench occurs and the current of the superconducting coils drops to 0 A as well. The loss of the electron beam is generated by sudden orbit oscillations observed along the ANKA storage ring. The orbit oscillations start 1 s before the start of the drop of the beam current, during the optics change performed to reduce the momentum compaction factor α_c. When the temperature at the liner downstream starts to increase the vertical orbit oscillations are strongly increased from few hundreds μm to few mm. The reason for the temperature increase is most likely due to a higher amount of synchrotron radiation hitting the liner on the upper surface, which is also where the temperature sensor is placed. To be noticed is that the data are logged with a time interval of 1 s. The temperature of the coils rises up to about 12 K in about 30 s. The SCU15 coils recover the operating temperature ca. 30 min after the quench, but could start to
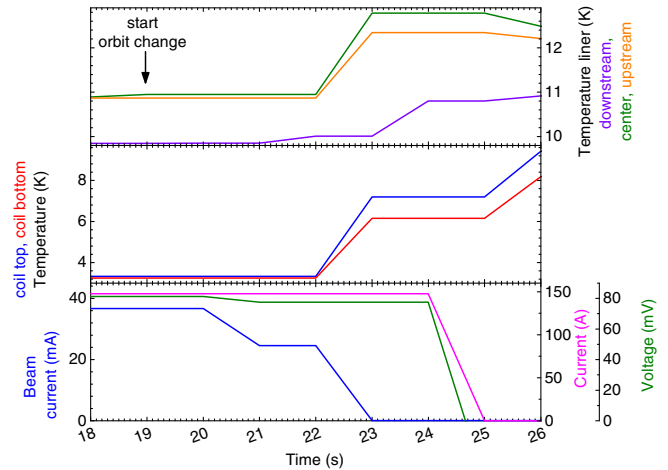

FIG. 13. The beam current, the current and voltage of the main coils of the SCU15 during a quench (lower plot), the temperatures of the SCU15 main coils (middle plot), and the temperatures of the SCU15 liner (upper plot) are plotted as a function of time.

be powered already after 15 min, when they reach 3.6 K (see Fig. 14).

Several third generation light sources offer low α_c operation mode [12,13] used for experiments with THz radiation and time resolved x-rays. For the application of SCUs in third generation light sources it is therefore essential to show that the SCU15 does not affect the low α_c mode operation, and at the same time that it can be operated in the low α_c mode, giving the possibility to use it to perform time resolved x-rays experiments. Despite the two occurrences, the SCU15 can be powered in this mode: while squeezing the beam, the liner temperature
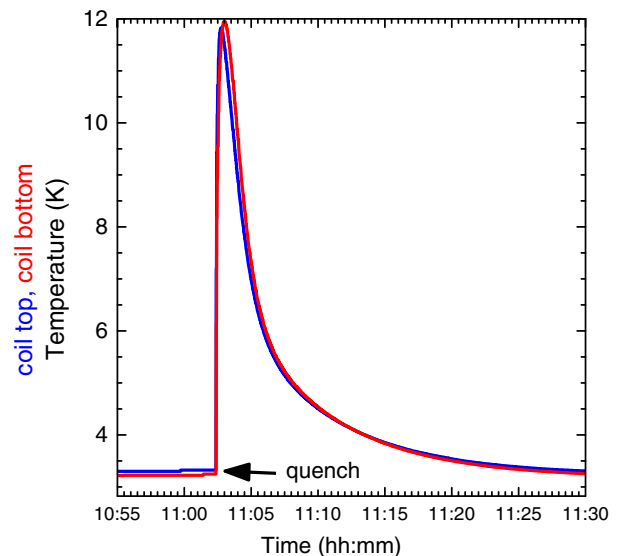

FIG. 14. Temperature of the top and bottom coils before and after a quench as a function of time.
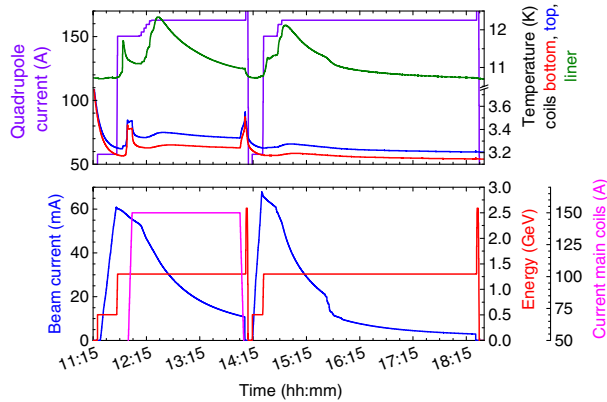
FIG. 15. Top. Current of the one of the quadrupole families (violet line) and the temperature of the top (blue line) and bottom (red line) coils as well as of the liner (green line) as a function of time. As the current of the quadrupole grows the beam gets shorter. Bottom. Beam parameters as a function of time: current (blue line), energy (red line), and current in the main coils (magenta line) of the SCU15. The SCU15 gap is open in the second run.

increases by 1.5 K, while the temperature of the coils does not increase more than 0.1 K. It could also be proven that the operation of the SCU15 does not change the low α_c mode operation. All this is demonstrated in Fig. 15, where the temperature of the top (blue line) and bottom (red line) coils as well as of the liner (green line) as a function of time are shown in the upper plot, and the beam parameters as well as the current in the main coils of the SCU15 as a function of time are shown in the lower plot. It can be seen that the beam is squeezed by the increase of the quadrupole current (see violet line in the upper plot of Fig. 15). The lifetime in the two runs is comparable.

VI. SPECTRAL CHARACTERIZATION

A. Experimental setup

The spectral characterization of the SCU15 has been performed with the setup schematically shown in Fig. 16. The synchrotron radiation emitted by the SCU15 passes through a Be window of 3 mm diameter and 0.5 mm thick, separating the ultra high vacuum of the storage ring from the one of the beam line. The window is motorized and surrounded by a water cooled oxygen free high thermal conductivity (OFCH) copper block. A tungsten pinhole of 50 μm diameter mounted on a water cooled copper block is used to fix the divergence of the x-ray beam. Afterwards, the photon beam hits a channel cut Si 111 monochromator selecting the energy of the radiation, and is then detected in the first ionization chamber (Oken Ltd, Japan). The two ionization chambers can be filled with different gases at a defined pressure in the range of 100–900 mbar. For the measurements of the SCU15 spectrum the ion chambers were filled with nitrogen at 900 mbar. Two kapton windows 75 μm thick allow the beam to pass each of the ionization chambers. While the first ionization chamber is used to detect the flux, the second one is used together with the filter carousel to calibrate the energy of the radiation selected by the monochromator. The carousel consists of a rotating wheel, containing several filters (Ag, Au, Bi, Cr, Ti, Ta) with absorption edges in the working range of the monochromator between 3 and 20 keV. It is also possible to let the radiation through without passing any filter. The energy of the radiation is selected by means of a Si 111 channel cut monochromator. Using the absorption edges of filters like Ta, it is possible to calibrate the Bragg angle to the corresponding energy within few eV, which is the width of the absorption edges. The following absorption edges have been used: L-I (11.682 keV), L-II (11.136 keV)
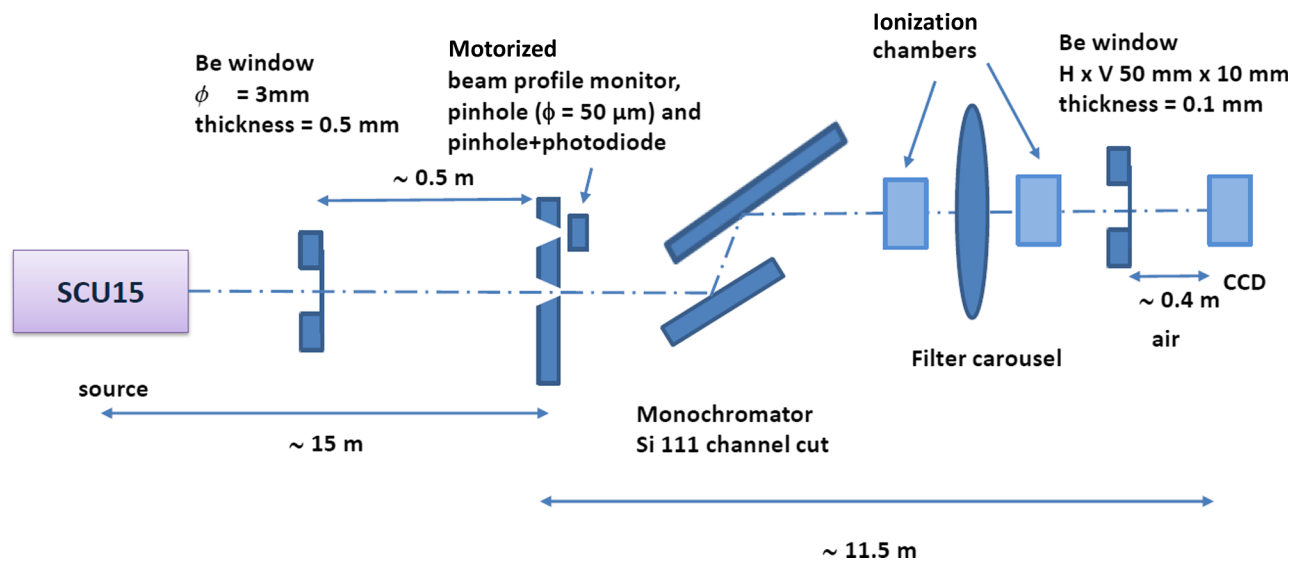

FIG. 16. Setup used at the ANKA storage ring for the spectral characterization of the SCU15.
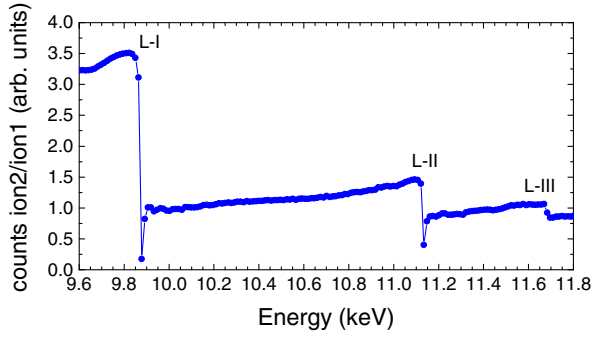
FIG. 17.   The counts of the second ionization chamber normalized to the counts of the first ionization chamber, showing the Ta absorption edges from the L shell, are plotted as a function of the photon energy, after calibration.

and L-III (9.881 keV) of Ta, and K-I (5.989 keV) of Cr [14]. The counts of the second ionization chamber normalized to the counts of the first ionization chamber, showing the Ta absorption edges from the L shell, are plotted as a function of the photon energy in Fig. 17, after calibration.

After the second ionization chamber the photon beam is transported in vacuum up to the second Be window 0.1 mm thick, 50 mm wide, and 10 mm high. The monochromatic beam passes then through about 0.4 m of air and can be detected by using a high resolution detector composed of a 50 μm thick LuAG:Ce scintillator, which is coupled to a CCD camera PCO.4000 via a diffraction limited monochromatic microscope [15]. The used magnification was 3.125x resulting in an effective pixel size of 2.88 μm. The field of view (FOV) that corresponds to the lowest magnification is 11.52 mm(H) $\times$ 7.68 mm(V). The integration time used to detect the x-ray image of the monochromatic beam was 20 s. The CCD camera has been used to measure the spatial distribution of the different harmonics.

The white beam power density spatial distribution can be measured using the photodiode installed behind the second pinhole of the beam profile monitor.

B. Spectrum

The measured flux of the SCU15 at the maximum operation current 150 A normalized to 100 mA electron beam current is shown in Fig. 18. The photon flux N, i.e., the number of photons per sec per 0.1% energy bandwidth $\Delta E/E$, generated by the SCU15 passing through a 50 μm diameter pinhole is given by [16]:

$$N = \exp(\mu_{Be})(CTS - \text{Noise})f_C \frac{100}{I_{\text{beam}}} \frac{0.001}{\Delta E/E}, \quad (2)$$

where $\exp(-\mu_{Be})$ is the transmission of the 0.5 mm thick Be window, being μ_{Be} its optical depth, CTS are the counts in the ionzation chamber, *Noise* are the counts measured in
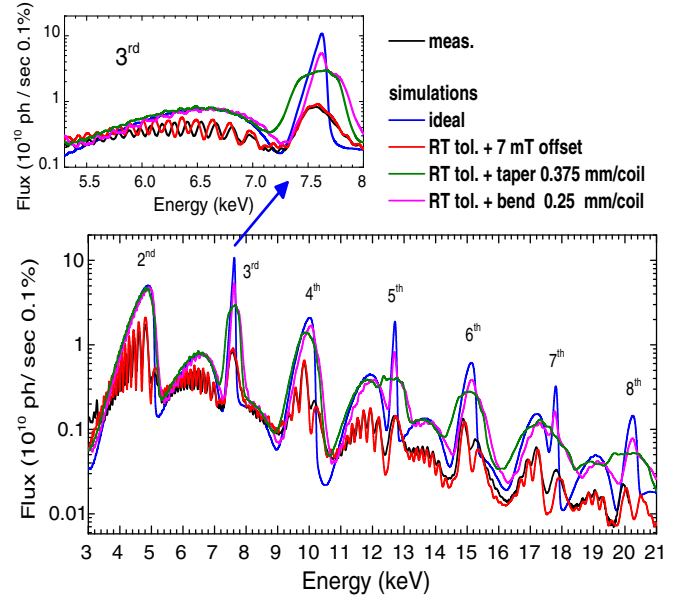

FIG. 18.   Flux generated by the SCU15 at the maximum operating current 150 A in the main coils, at 2.5 GeV and normalized to 100 mA, through a pinhole of 50 μm diameter at 14.9 m, measured with a channel cut Si 111 monochromator and the first ionization chamber, as described in the previous subsection (black line). The measured flux is compared with the ones using as input a magnetic field generated with FEMM (Finite Element Method Magnetics) adopting a geometry that takes into account the mechanical variations of the half period length and pole height measured at room temperature along each coil (RT tol.) with an offset of 7 mT (red line), with a tapering of 0.375 mm/coil (olive line), and with a bending of 0.250 mm/coil (magenta line). The spectrum of an ideal field with 0.73 T peak field on axis is also reported (blue line).

the ionization chamber without photon beam, f_C is the ionization chamber conversion factor given by the ratio of the photons impinging in the detector and the corresponding CTS, and I_{beam} is the electron beam current in mA. The ionization chamber conversion factor f_C depends on several factors including the length of the ionization chamber, the kind of gas with which it is filled and its pressure [17]. The energy bandwidth is determined by:

$$\Delta E/E = \cot \theta_B \sqrt{\omega^2 + \Delta \theta^2} \quad (3)$$

being θ_B the Bragg angle, ω the intrinsic angular width of diffraction (Darwin width), and $\Delta \theta$ the beam divergence defined by the pinhole aperture and its distance from the source. The Darwin width of the Si 111 crystal has been calculated using the free software provided by S. Stepanov [18]. The transmission $\exp(-\mu_{Be})$, the ionization chamber conversion factor f_C, and the Darwin width ω are functions of the photon energy (see Appendix).

The spectrum measured at different currents of the SCU15, as well as the white beam profile measured with the photodiode placed behind the beam profile monitor are reported in Ref. [19].
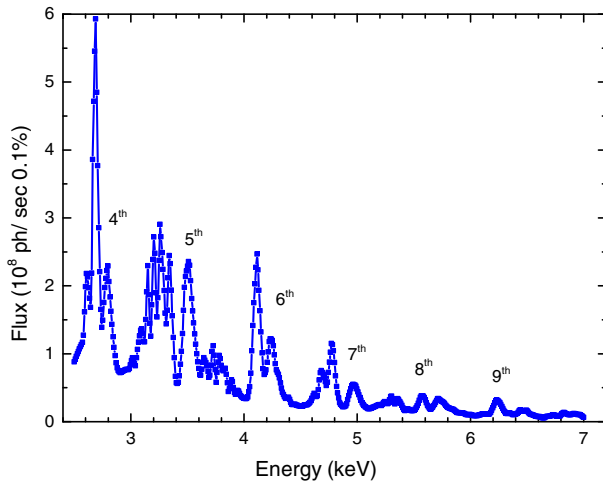
FIG. 19.   Flux generated by the SCU15 at the maximum operating current 150 A in the main coils, at 1.3 GeV and normalized to 100 mA, through a pinhole of 50 μm diameter at 14.9 m, measured with a channel cut Si 111 monochromator and the first ionization chamber, as described in the previous subsection.

The spectrum measured at 1.3 GeV, showing the capabilities of the SCU15 at ANKA in the low α_c mode, is shown in Fig. 19.

As mentioned in Sec. II, the windings in the last groove of one of the main coils have been bypassed while repairing the coils during assembly. As a consequence, the first and second field integral are not compensated, and a constant field along the coils is generated due to the asymmetry in the first and last groove, and to the presence of the iron yoke (iron also below the winding packages). This has been confirmed by local magnetic field measurements performed in LHe and the facility CASPER II on a SCU mockup 30 cm long and with 20 mm period length [20], where a different number of windings was present in the first and last groove of one of the coils. A constant field is not expected in case of an asymmetry in the end magnets of a hybrid permanent magnet undulator, where only iron poles are present. Simulations with FEMM [21] (2D) using only coils and iron poles without an iron yoke confirmed this. However, the models for the magnetic structure used in FEMM and Radia [22] are respectively 2D and quasi-3D, and do not quantitatively predict the end fields, while they can nicely reproduce the local and long range variations of the field along the coil (except the first and last periods). For this reason, in order to simulate the spectra from a specific magnetic field configuration we used the results from the programs mentioned above, and added a constant field instead of removing the windings in the last groove of one of the coils.

The spectra presented in the following have been simulated with the free software SPECTRA [23], using the ANKA beam parameters: beam energy 2.478 GeV [24], beam current 100 mA, energy spread 0.001, horizontal emittance 41 nm rad, vertical emittance 0.3 nm rad, horizontal beta function 19 m, and vertical beta function 1.7 m.
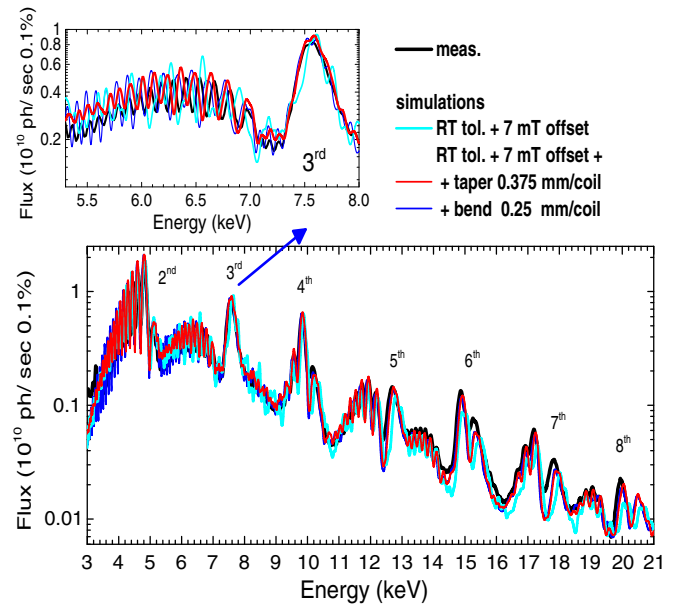

FIG. 20.   The measured flux (black line) is compared with the ones using as input a magnetic field generated with FEMM adopting a geometry that considers the mechanical variations of the half period length and pole height measured at room temperature along each coil (RT tol.) and an offset of 7 mT (red line), as well as by the field obtained including a tapering of 0.375 mm/coil (cyan line), and by including a bending of 0.250 mm/coil (blue line).

The presence of a constant magnetic field along the coils is the main reason for the observed degradation of the spectrum, caused by a bending of the electron trajectory. The peaks of the odd harmonics are substantially reduced from the ideal case. This can be observed in Fig. 18, where the measured spectrum is compared to the ideal case with a peak field of 0.73 T and to a spectrum simulated using as input a magnetic field generated with FEMM adopting a geometry that takes into account the half period length and pole height variations measured for the 2 coils at room temperature [9] (in the figures referred to as 'RT tol.', see also Sec. II) with an offset of 7 mT. The wiggling observed on the rising edge of the second harmonic and in the region with smaller energies than the peak in the odd harmonics is also evidence of an offset in the magnetic field on axis. A wiggling at the lower energy side of the first harmonic as a consequence of a dipole field component added to an ideal undulator field is predicted also in Ref. [25]. A small horizontal field component due to a possible misalignment between the 2 undulator coils and/or to a misalignment of the magnetic plane with respect to the orbit plane, can also contribute to the degradation of the spectrum. A misalignment of the magnetic plane with respect to the orbit plane can be corrected: the SCU15 has a motorized support structure which allows us to optimize the alignment while the storage ring is in operation. From the orbit measurements performed in the ANKA storage ring we can limit the
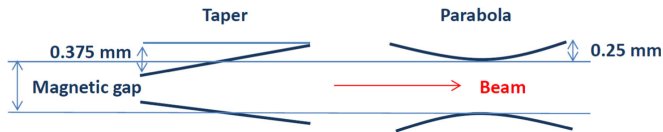
FIG. 21. A sketch of the geometry of the taper and parabola long range deviations used as input in FEMM to simulate the magnetic field for the spectral simulations presented in Figs. 18 and 20.

contribution of a constant horizontal field to about 1 μT. The degradation of the ideal spectrum from such a constant horizontal field component is smaller than what caused by the mechanical accuracies measured at room temperature, and has therefore been neglected in the following analysis. In addition to the offset in the magnetic field, the coils could present a bending, as observed in the local field measurements performed in a LHe bath at CERN [9], and/or a tapering possibly caused by a misalignment of the coils during assembly in the final cryostat. Before installation in the final cryostat the coils have been prebent to compensate the bending of 0.25 mm/coil observed in the measurements performed at CERN. However, the magnetic field profile has not been measured afterward. In order to distinguish between the different contributions to the spectrum we have compared to the measured one, the spectra simulated using as input the magnetic field profile obtained by FEMM simulations with a geometry considering the mechanical variations of the half period length and pole height measured at room temperature along each coil (RT tol.): (i) with an offset in the magnetic field on axis of 7 mT, (ii) with a taper of 0.375 mm/coil, corresponding to a gradient of -0.05 T/m, (iii) with a bending of 0.25 mm/coil, which corresponds to a maximum decrease in the peak field of 50 mT from the peak field 0.73 T. A sketch of the geometry used as input in FEMM to simulate the taper and parabola long range deviations for the simulations mentioned above is shown in Fig. 21. The magnetic field profiles are, without considering the offset, all normalized to have 0.73 T in the middle of the undulator. This comparison, shown in Fig. 18 together with the spectrum of an ideal field with peak field on axis of 0.73 T, demonstrates that the main reason of the reduction of the flux observed is caused by the presence of an offset in the magnetic field profile along the coils, generated by the bypass of the windings in the last groove of one of the coils.

From the comparison of the measured and simulated flux around the peak of the third harmonic using an ideal field varying from 0.725 T and 0.735 T and an offset of 7 mT, we infer a peak field on axis of 0.732 ± 0.002 T.

In order to understand if it is possible to recover the mechanical tolerances reached in cold conditions by the coils by means of the measured spectrum and flux spatial distribution at fixed energies, several magnetic field simulations with FEMM have been performed considering the mechanical accuracies measured at room temperature (about 50 μm, see Sec. II) together with long range

deformations caused by misalignment (tapering) and by cooling (bending), as observed in the measurements performed in a LHe bath at CERN (0.25 mm/coil). Several field distributions have been simulated varying the tapering and bending deformations in steps. For the tapering the following values have been considered: ± 0.05 mm/coil, ± 0.1 mm/coil, ± 0.15 mm/coil and ± 0.375 mm/coil (for a negative tapering, i.e., -0.375 mm/coil, the beam sees at the entrance of the undulator the largest gap); while for the bending: 0.05 mm/coil, 0.1 mm/coil, 0.15 mm/coil and 0.25 mm/coil. The simulated field, always adding the offset generated by bypassing the windings in the last groove of one of the main coils, has been used as input to simulate the spectrum and the flux density spatial distribution at fixed energies with SPECTRA. Those simulations have been compared with the measured spectrum and flux density spatial distribution measured with the CCD camera. From the comparison between the measured spectrum and the simulated ones it is not possible to constrain the maximum tapering and bending of the coils. The reason is that the shape of the spectrum is dominated by the effect of the offset. The measured spectrum is well reproduced by the simulations using as input the field obtained considering the variations of the half period length and pole height measured at room temperature along each coil (RT tol.) and an offset of 7 mT, as well as by the field obtained including a tapering of 0.375 mm/coil, and by including a bending of 0.25 mm/coil (see Fig. 20). In order to constrain the maximum tapering and bending of the coils, we use the comparison of the simulations with the measured flux spatial distribution at fixed energies around the "exact" third harmonic at 7800 eV, which is at half of the total flux [26]. Around 7800 eV the horizontal profile of the flux is very sensitive to the interference effects and as a consequence to the variations of the field profile from the ideal case, depending on the mechanical tolerances reached in cold conditions. The comparison is shown in Fig. 22. Only the flux density spatial distribution simulated using a magnetic field profile including the mechanical tolerances measured at room temperature, an offset of 7 mT and a bending of 0.05 mm/coil shows a similar behavior to the measured one: the observed maximum along the horizontal axis shifts horizontally. The dashed ellipses on the simulations indicate the projections of the Be window on the CCD. Of all the simulations performed that have been mentioned above, varying the bending and the tapering of the coils, only with a bend of 0.05 mm/coil it is possible to reproduce, at least qualitatively, the behavior observed of the horizontal shift of a peak by changing the energy. The measured horizontal profiles at $y = 3.7$ mm and the simulated ones at $y = 0$ mm for the case of a bending of 0.05 mm/coil, filtered with a transmission function and normalized to the maximum measured counts, show a
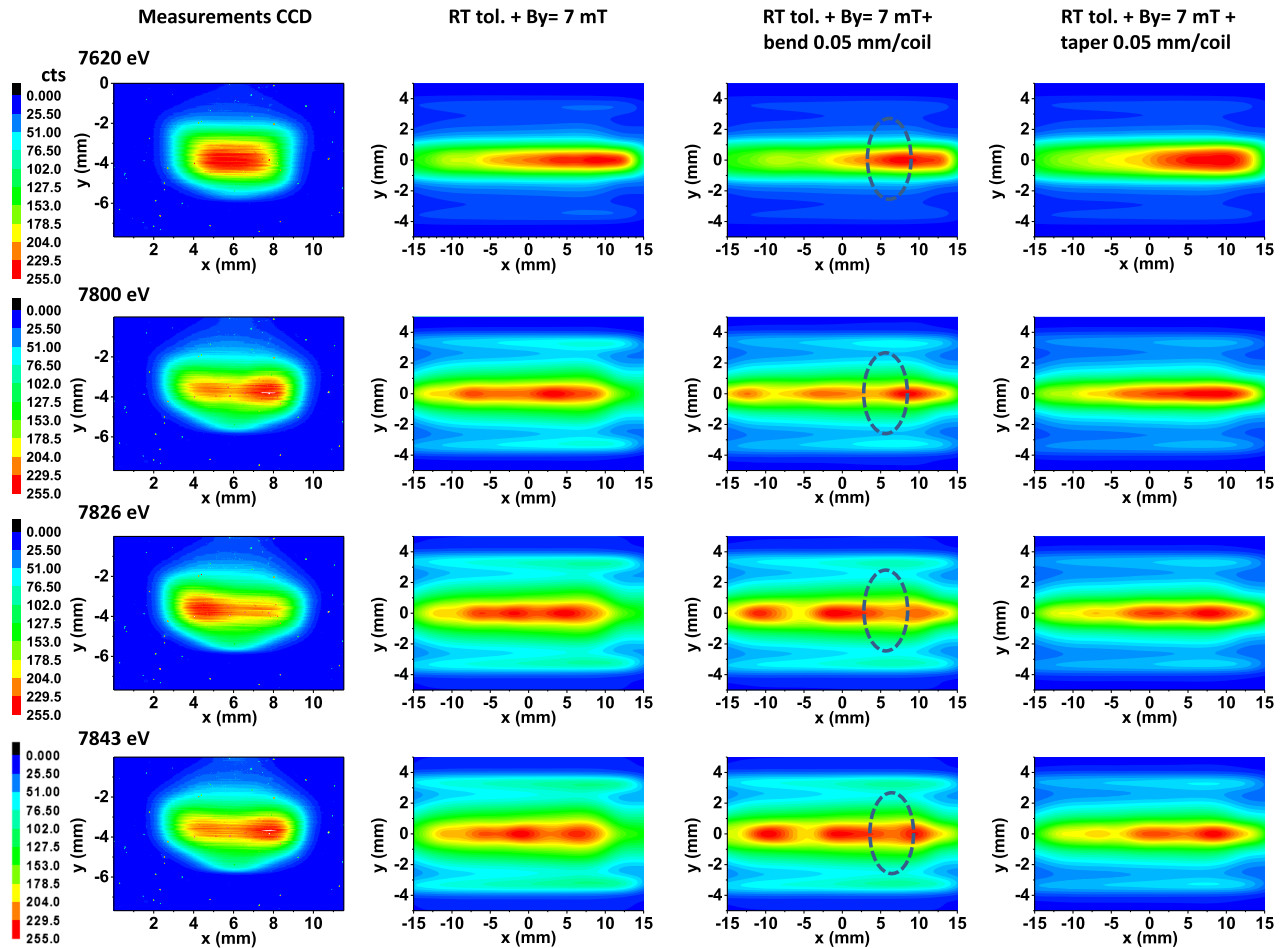
FIG. 22.   Spatial distribution of the flux density generated by the SCU15 at the maximum operating current 150 A in the main coils, at 2.5 GeV measured with a CCD camera at 26 m from the source (SCU15), as described in the previous subsection (first column) at 4 different photon energies on the falling flank of the third harmonic. The measured flux is compared with the ones simulated using as input a magnetic field generated with FEMM adopting a geometry that considers the mechanical variations of the half period length and pole height measured at room temperature along each coil (RT tol.) and an offset of 7 mT (second column), as well as by the field obtained including a tapering of 0.05 mm/coil (third column), and by including a bending of 0.05 mm/coil (fourth column).

qualitative agreement (see Fig. 23). We would then conclude that the prebending performed during assembly to compensate the 0.25 mm bend/coil measured at CERN in a LHe test bath nicely worked out. The long range bending of 0.05 mm/coil is of the same order of the mechanical tolerances measured at room temperature. The expected spectrum from the reached mechanical tolerances in cold conditions including the windings in the last groove of one of the coils (not considering the offset of 7 mT in the magnetic field profile) is shown in Fig. 24. This is here compared with the ideal case, with the simulated one considering the offset of 7 mT and with the measured spectrum. The results are quite encouraging, since they show that removing the bypass of the windings in the last groove of one of the coils a spectrum very close to the ideal one could be reached without applying local shimming.
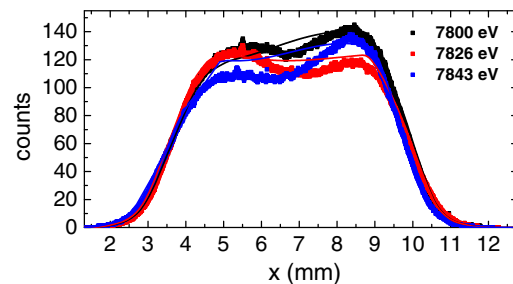

FIG. 23.   Horizontal profiles from the measured (squares) and simulated (lines) flux density distribution at 3 fixed energies on the falling flank of the third harmonic: 7800 eV (black), 7826 eV (red), and 7843 eV (blue). The measured horizontal profiles are extracted at $y = 3.7$ mm from the first column and the simulated ones at $y = 0$ mm from the third column of Fig. 22.
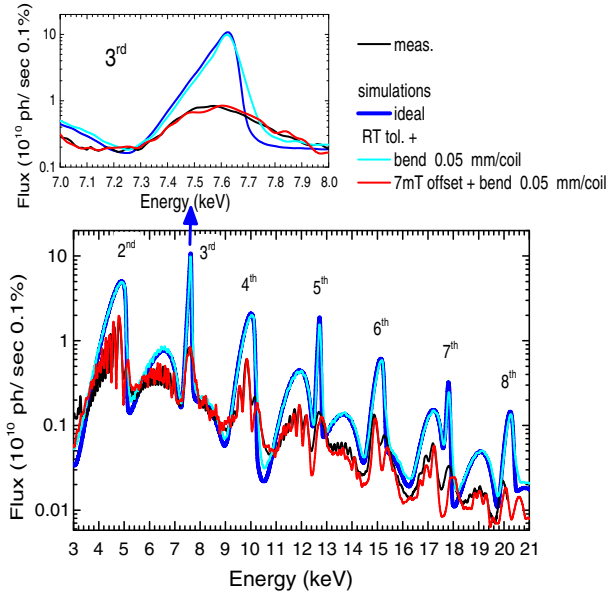
FIG. 24. The measured flux (black line) is compared with the ones simulated considering an ideal case with 0.73 T peak field (blue line), as well as with the ones using as input a magnetic field generated with FEMM adopting a geometry that considers the mechanical variations of the half period length and pole height measured at room temperature along each coil (RT tol.) and a bend of 0.05 mm/coil with (red line) and without an offset of 7 mT (cyan line).

VII. CONCLUSIONS

A full length SCU (1.5 m long coils) with a period length of 15 mm, conduction cooled and with a variable gap, has been successfully developed and tested in the ANKA storage ring. A reliable and safe operation without quenches has been demonstrated while operating the ring at 2.5 GeV. The SCU15 reaches, while in operation with beam, despite the beam heat load, a higher peak field on axis than the one reachable with an ideal CPMU with the same geometry. This is made possible by minimizing the difference between magnetic and vacuum gap to 1 mm and keeping a good thermal decoupling between the coils (∼4 K) and the liner (∼10 K), separated by 0.2 mm along 1.5 m distance.

The SCU15 could also be operated in the low α_c momentum compaction mode without changing this operation mode of the storage ring, used in third generation light sources for experiments with THz radiation and time resolved X-rays.

Unfortunately, a bypass of the windings in the last groove of one of the coils substantially reduces the spectral performance of the SCU15 with respect to the ideal case. We could however show, that if the bypass would be removed, since the deformation reached in cold conditions are in the order of 0.05 mm, it would be possible to reach a spectrum very close to the ideal one (see Fig. 24) without applying local shimming.

The lessons learned with the SCU15 are applied to the next SCU under development, a full scale device (1.5 m long coils) with 20 mm period length, for which the aim is to demonstrate a better spectral performance than with CPMUs.

The installation, the reliable operation and all the results from the cold tests of the SCU15 with and without beam are very encouraging for the future implementation of SCUs in running and planned low emittance light sources.

APPENDIX:

We report here the transmission $\exp(-\mu_{\mathrm{Be}})$ (see top Fig. 25), the ionization chamber conversion factor f_C given
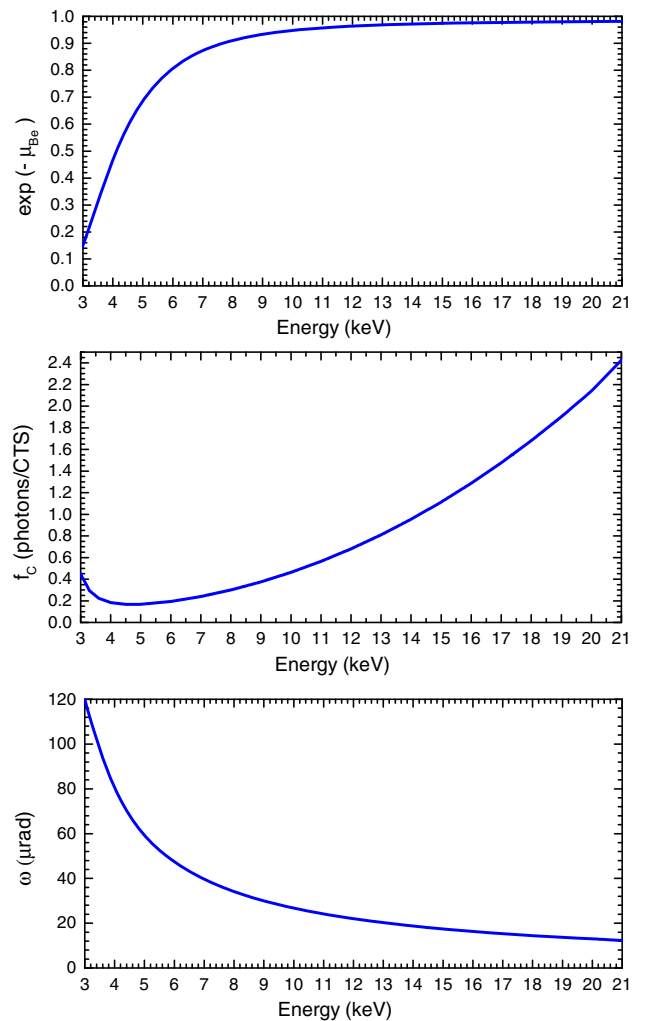

FIG. 25. Top. Transmission of the 0.5 mm thick Be window as a function of energy [23]. Middle. Ionization chamber conversion factor f_C as a function of energy [17]. Bottom. Darwin width ω of the Si111 crystal as a function of energy [18].

by the ratio of the photons impinging in the detector and the corresponding measured counts (see middle Fig. 25), and the Darwin width ω of the Si111 crystal (see bottom Fig. 25) as functions of the photon energy, used in Eq. (2) to calculate the photon flux from the measured counts in the first ionization chamber.

[1] J. Clarke and T. Bradshaw, https://eventbooking.stfc.ac.uk/uploads/scu-workshop-report.pdf.

[2] H. O. Moser, B. Krevet, and H. Holzapfel, Patent DE 4101094 C1 (1991).

[3] S. Casalbuoni, M. Hagelstein, B. Kostka, R. Rossmanith, M. Weisser, E. Steffens, A. Bernhard, D. Wollmann, and T. Baumbach, Generation of x-ray radiation in a storage ring by a superconductive cold-bore in-vacuum undulator, Phys. Rev. ST Accel. Beams **9,** 010702 (2006).

[4] Y. Ivanyushenkov *et al.*, Development and operating experience of a short-period superconducting undulator at the Advanced Photon Source, Phys. Rev. ST Accel. Beams **18,** 040703 (2015).

[5] M. E. Couprie *et al.*, The LUNEX5 project in France, FLS'12, Newport News, VA, USA (2012), https://www.jlab.org/conferences/FLS2012/talks/Mon/Lunex5_FLS2012-WGFEL.pdf.

[6] C. Boffo, W. Walter, T. Baumbach, S. Casalbuoni, S. Gerstl, A. Grau, M. Hagelstein, and D. Saez de Jauregui, The New Conduction-Cooled Superconducting Undulator for ANKA, IEEE Trans. Appl. Supercond. **21,** 1756 (2011).

[7] http://www.shicryogenics.com/products/4k-cryocoolers/.

[8] S. Casalbuoni, A. Grau, M. Hagelstein, R. Rossmanith, F. Zimmermann, B. Kostka, E. Mashkina, E. Steffens, A. Bernhard, D. Wollmann, and T. Baumbach, Beam heat load and pressure rise in a cold vacuum chamber, Phys. Rev. ST Accel. Beams **10,** 093202 (2007).

[9] S. Casalbuoni, T. Baumbach, S. Gerstl, A. Grau, M. Hagelstein, D. Saez de Jauregui, C. Boffo, J. Steinmann, and W. Walter, Training and magnetic field measurements of the ANKA superconducting undulator, IEEE Trans. Appl. Supercond. **21–3,** 1760 (2011).

[10] P. Nagel (private communication).

[11] A.-S. Müller, I. Birkel, B. Gasharova, E. Huttel, R. Kubat, Y.-L. Mathis, D. A. Moss, W. Mexner, R. Rossmanith, M. Wuensch, P. Wesolowski, F. Pérez, M. Pont, and C. J. Hirschmugl, Far Infrared Coherent Synchrotron Edge Radiation at ANKA, in *Proceedings of the 21st Particle Accelerator Conference, Knoxville, TN, 2005* (IEEE, Piscataway, NJ, 2005), p. 2518.

[12] M.-A. Tordeux, J. Barros, A. Bence, P. Brunelle, N. Hubert, M. Labat, A. Nadji, L. Nadolski, P. Lebasque, and J.-P. Pollina, Low-alpha Operation for the SOLEIL Storage Ring, in *Proceedings of the 3rd International Particle Accelerator Conference, New Orleans, LA, 2012* (IEEE, Piscataway, NJ, 2012), p. 1608.

[13] I. P. S. Martin, R. Bartolini, G. Rehm, J. H. Rowland, and C. Thomas, Low Alpha Operation of the Diamond Storage Ring, in *Proceedings of the International Particle Accelerator Conference, Kyoto, Japan* (ICR, Kyoto, 2010), p. 4599.

[14] A. C. Thompson *et al.*, *X-Ray Data Booklet, Center for X-ray Optics and Advanced Light Source*, 3rd ed., Lawrence Berkeley Laboratory (University of California, Berkeley, 2009).

[15] P. A. Douissard, A. Cecilia, X. Rochet, X. Chapel, T. Martin, T. van de Kamp, L. Helfen, T. Baumbach, L. Luquot, X. Xiao, J Meinhardt, and A. Rack, A versatile indirect detector design for hard X-ray microimaging, J. Instrum. **7,** P09016 (2012).

[16] M. Sanchez del Rio and O. Mathon, A simple formula to calculate the x-ray flux after a double-crystal monochromator, Proc. SPIE Int. Soc. Opt. Eng. **5536,** 157 (2004).

[17] J. Tischler, http://sector34.xray.aps.anl.gov/tischler/igor/index.html.

[18] http://sergey.gmca.aps.anl.gov/x0h.html.

[19] S. Casalbuoni, A. Cecilia, S. Gerstl, N. Glamann, A. Grau, T. Holubek, C. Meuter, D. Saez de Jauregui, R. Voutta, C. Boffo, Th. Gerhard, M. Turenne, and W. Walter, Overview of the superconducting undulator development program at ANKA, AIP Conf. Proc. **1741,** 020002 (2016).

[20] A. Grau, S. Casalbuoni, S. Gerstl, N. Glamann, T. Holubek, D. Saez de Jauregui, R. Voutta, C. Boffo, Th. Gerhard, M. Turenne, and W. Walter, Characterization of 30-cm-long superconducting undulator coils with the magnetic measurement system CASPER II, IEEE Trans. Appl. Supercond. **26–4,** 4100804 (2016).

[21] D. Meeker, Finite element method magnetics, http://www.femm.info/wiki/HomePage.

[22] O. Chubar, P. Elleaume, and J. Chavanne, A three-dimensional magnetostatics computer code for insertion devices, J. Synchrotron Radiat. **5,** 481 (1998).

[23] T. Tanaka and H. Kitamura, SPECTRA: a synchrotron radiation calculation code, J. Synchrotron Radiat. **8,** 1221 (2001).

[24] A.-S. Müller, I. Birkel, E. Huttel, F. Perez, M. Pont, and R. Rossmanith, Energy Calibration of the ANKA Storage Ring, in *Proceedings of the 9th European Particle Accelerator Conference, Lucerne, 2004* (EPS-AG, Lucerne, 2004), p. 2311 [http://accelconf.web.cern.ch/AccelConf/e04/].

[25] M. Homscheidt, Master Thesis, University of Karlsruhe, Karlsruhe, Germany, 1999.

[26] J. Clarke, *The Science and Technology of Undulators and Wigglers* (Oxford University Press, New York, 2004).